

MASS-GAP MERGERS IN ACTIVE GALACTIC NUCLEI

HIROMICHI TAGAWA¹, BENCE KOCSIS², ZOLTÁN HAIMAN³, IMRE BARTOS⁴, KAZUYUKI OMUKAI¹, JOHAN SAMSING⁵¹Astronomical Institute, Graduate School of Science, Tohoku University, Aoba, Sendai 980-8578, Japan²Rudolf Peierls Centre for Theoretical Physics, Clarendon Laboratory, Parks Road, Oxford OX1 3PU, UK³Department of Astronomy, Columbia University, 550 W. 120th St., New York, NY, 10027, USA⁴Department of Physics, University of Florida, PO Box 118440, Gainesville, FL 32611, USA⁵Niels Bohr International Academy, The Niels Bohr Institute, Blegdamsvej 17, 2100 Copenhagen, Denmark*Draft version May 28, 2022*

ABSTRACT

The recently discovered gravitational wave sources GW190521 and GW190814 have shown evidence of BH mergers with masses and spins that could be outside of the range expected from isolated stellar evolution. These merging objects could have undergone previous mergers. Such hierarchical mergers are predicted to be frequent in active galactic nuclei (AGN) disks, where binaries form and evolve efficiently by dynamical interactions and gaseous dissipation. Here we compare the properties of these observed events to the theoretical models of mergers in AGN disks, which are obtained by performing one-dimensional N -body simulations combined with semi-analytical prescriptions. The high BH masses in GW190521 are consistent with mergers of high-generation (high-g) BHs where the initial progenitor stars had high metallicity, 2g BHs if the original progenitors were metal-poor, or 1g BHs that had gained mass via super-Eddington accretion. Other measured properties related to spin parameters in GW190521 are also consistent with mergers in AGN disks. Furthermore, mergers in the lower mass gap or those with low mass ratio as found in GW190814 and GW190412 are also reproduced by mergers of 2g-1g or 1g-1g objects with significant accretion in AGN disks. Finally, due to gas accretion, the massive neutron star merger reported in GW190425 can be produced in an AGN disk.

Keywords: binaries: close – gravitational waves – galaxies: active – methods: numerical – stars: black holes

1. INTRODUCTION

Recently, several gravitational wave (GW) events were reported by LIGO and Virgo whose measured physical properties pose interesting constraints on their astrophysical origin. One of these is GW190521 (The LIGO Scientific Collaboration et al. 2020b; Abbott et al. 2020d), in which the masses of the merging BHs ($85^{+21}_{-14} M_{\odot}$ and $66^{+17}_{-18} M_{\odot}$, but see Nitz & Capano 2020) indicate that the merging BHs fall into the so-called “upper-mass gap”, as they are heavier than the maximum BH mass imposed by (pulsation) pair-instability supernovae (Chatzopoulos & Wheeler 2012; Farmer et al. 2019). The components’ dimensionless spins ($a = 0.69^{+0.27}_{-0.62}$ and $0.73^{+0.24}_{-0.64}$) are also larger than the maximum natal spins predicted by stellar evolutionary models for angular momentum transfer (Fuller & Ma 2019). A possible electromagnetic counterpart has been reported for GW190521, which, if real, would suggest mergers in gas-rich environments (McKernan et al. 2019; Graham et al. 2020). Further candidates for mergers in the upper-mass gap are reported in GW170729 (Abbott et al. 2019), GW170817A (Zackay et al. 2019a), and six other candidates in O3 (Abbott et al. 2020c).

Similarly, the neutron star (NS) merger GW190425 indicates masses higher than in NS binaries observed in the Milky Way (Abbott et al. 2020a). Additionally, mergers with very unequal masses have been reported – GW190412 (The LIGO Scientific Collaboration et al. 2020a) and GW190814 (Abbott et al. 2020b) –, which are also atypical in stellar evolutionary models of isolated

binaries. The mass of the secondary object of $2.6 M_{\odot}$ in GW190814 falls in the so-called lower mass gap, predicted by stellar-evolutionary models (Fryer et al. 2012) and obeyed by observations of X-ray binaries (Özel et al. 2012). The object in the lower mass gap in GW190814 and a non-zero spin for the primary BH ($0.43^{+0.16}_{-0.26}$) in GW190412 are consistent with a scenario in which the merging compact objects (COs) had experienced previous mergers or significant accretion. These events suggest that growth by gas accretion or hierarchical mergers may be common among COs (see e.g. O’Leary et al. 2016; Gerosa et al. 2020b; Abbott et al. 2020d; Safarzadeh & Haiman 2020). By analyzing the ensemble of events detected during LIGO/Virgo’s O1-O3a observing runs, Kimball et al. (2020) and Tiwari & Fairhurst (2020) found preference for at least one, but probably multiple hierarchical mergers in the detected sample. The results by Kimball et al. (2020) strongly depend on the escape velocity at the merger sites, with higher escape velocities favoring a larger number of hierarchical mergers.

Active galactic nuclei (AGNs) represent environments where mass growth by gas accretion is possible (Levin 2007) and hierarchical mergers are frequent due to efficient hardening by interaction with gas (e.g. Bartos et al. 2017; Stone et al. 2017; McKernan et al. 2018), stars, and COs (Tagawa et al. 2020b, hereafter Paper I). Additionally, the high escape velocity in such systems helps retain recoiling merger remnants. Yang et al. (2020a) investigated the possibility of lower mass gap mergers by assuming that the objects are quickly delivered to migration traps of AGN disks where they undergo mergers. In Paper I, we performed one-dimensional (1D) N -body

simulations combined with semi-analytical prescriptions for gaseous and stellar effects, to follow the evolution of binary separation, along with the radius and inclination of the orbit around the SMBH. The results showed that binaries form efficiently during dynamical encounters in gas, and mergers are facilitated by binary-single (BS) interactions in the gap-forming inner regions. In Tagawa et al. (2020a, hereafter Paper II), we extended this model to follow the evolution of BH spins, and binary orbital angular momentum directions. In Tagawa et al. (2020c, hereafter Paper III), we also included the effects of binary eccentricity, and found that mergers are often highly eccentric in AGN disks if BS interactions are confined to the AGN plane due to gaseous torques (see also Samsing et al. 2020) or if the objects migrate close to the SMBH where they undergo GW capture events.

In this *Letter*, we extend our previous models to include NSs. We then examine the mass distribution of merging binaries in the AGN channel, and assess the likelihood of mergers in the lower and upper mass gaps, those with highly unequal mass ratios, and massive NS mergers as seen in GW190521, GW190814, GW190412, and GW190425.

2. METHOD

Our model is based on Papers I, II, and III, summarized in § 2.1, with new ingredients described in § 2.2.

2.1. Overview of model

We consider a model with a supermassive BH (SMBH) at the center of a galaxy, surrounded by a gaseous accretion disk (hereafter AGN disk) and a spherical nuclear star cluster (NSC), which are assumed to be in a fixed steady-state. We follow the N -body evolution of COs consisting of those in the nuclear stars cluster and those captured inside the AGN disk.

We follow several pathways to form binaries. Some fraction of COs are initially in binaries. In the AGN disk, binaries form due to gas dynamical friction during two-body encounters and dynamical interactions during three-body encounters. Highly eccentric CO binaries also form due to the GW-capture mechanism in single-single encounters (e.g. O’Leary et al. 2009) and BS exchange interactions (Paper III).

Regarding the interaction with gas, the velocities of all COs relative to the local AGN disk decrease due to accretion torque and gas dynamical friction. The binaries’ semi-major axis decreases due to gas dynamical friction from the AGN disk. Their semi-major axis and eccentricity evolve also due to type I/II migration torque from a circumbinary disk. COs migrate toward the SMBH due to type I/II torques from the AGN disk. CO masses, BH spins, and the orbital angular momentum directions of binaries gradually evolve due gas accretion (Paper II).

We also account for dynamical interactions with single stars/COs and CO binaries. The binaries’ semi-major axis, velocities, orbital angular momentum directions, and eccentricity evolve due to BS interactions as prescribed in Leigh et al. (2018), and the velocities of all COs additionally evolve due to scattering. The soft binaries, i.e. those with binding energy lower than that of scattering objects, are either softened or ultimately disrupted during BS interactions. Hard binaries become

harder during BS interactions, and exchange interactions may take place; the most massive pair is assumed to remain in the binary after the interaction (Paper III).

The binaries’ separation and eccentricity decrease due to GW emission. When the pericenter distance of the binary becomes smaller than the innermost stable orbit, we assume that BHs merge, assign a kick velocity and mass loss due to GW emission, and prescribe BH spin evolution at the merger as in Paper II.

2.2. Evolution of neutron stars

While only stellar-mass BHs are followed in Papers I/II/III, here we additionally follow the evolution of NSs among the N -body particles. We assume that stars with zero-age main-sequence masses of $8\text{--}20\,\text{M}_\odot$ form NSs with $1.3\,\text{M}_\odot$. There are initially 5×10^4 NSs in the fiducial model. As NSs are lighter than BHs, we assume a shallower radial density profile

$$\frac{dN_{\text{NS,ini}}(r)}{dr} \propto r^{-0.5}, \quad (1)$$

where $N_{\text{NS,ini}}(r)$ is the total initial number of NSs within distance r from the central SMBH, and a higher velocity dispersion in the frame comoving with the AGN ($\sigma_{\text{NS}} = 0.4v_{\text{kep}}(r)$, where $v_{\text{kep}}(r)$ is the Keplerian velocity at r) compared to those for BHs ($dN_{\text{BH,ini}}(r)/dr \propto r^0$, $\sigma_{\text{BH}} = 0.2v_{\text{kep}}(r)$), as expected from relaxation processes (Hopman & Alexander 2006; Szolgyen & Kocsis 2018). For simplicity, we assume that the spin magnitudes of NSs are always zero, the mass lost during mergers is $0.01\,\text{M}_\odot$, and their radius is 10 km, within which NSs are assumed to merge in addition to the condition described above. We regard objects with mass less than $2\,\text{M}_\odot$ to be NSs, while we call objects with masses in the range $2\text{--}5\,\text{M}_\odot$ *lower mass gap objects* (LGOS), and treat LGOS as BHs in the calculations. We assign no kicks during NS-CO mergers for simplicity (but see Dietrich et al. 2017), while the spin evolution during NS-CO mergers is prescribed as for BH-BH mergers but with zero spin magnitudes for NSs. The interactions of NSs with gas, COs, and stars are prescribed in the same manner as for BHs.

2.3. Numerical choices

The parameters of the fiducial model (M1) are listed in Table 3 in the Appendix, which are the same as those in Papers I/II/III. We also study the additional models M2 and M3, which differ in the initial masses of stellar-mass BHs and efficiency of gas accretion.

In model M1, we set the mass of first-generation (1g) BHs to $m_{1g\text{BH}} \leq 15\,\text{M}_\odot$ given the observed high metallicity population for 90% of stars in the Milky Way NSC (e.g. Do et al. 2020) and the observations indicating strong mass loss during the luminous blue variable phase of solar-metallicity stars (e.g. Chen et al. 2015), which likely limits the maximum mass of 1g BHs to be $\sim 15\,\text{M}_\odot$ (e.g. Belczynski et al. 2010).

On the other hand, in model M2, the initial masses of 1g BHs are multiplied by 3 compared to the values in model M1, and so $m_{1g\text{BH}} \leq 45\,\text{M}_\odot$. Such high masses for 1g BHs may exist as indicated by a moderately metal-poor subpopulation in the Milky Way’s NSC (Do et al. 2020), and given that there are significant uncertainties in the initial mass function of 1g BHs in NSCs due to

Table 1

The results of different models at $t = 10$ Myr. The two leftmost ("input") columns show the model number and the differences from the fiducial model. The "output" columns list the fraction of mergers weighted by the detectable volume for BH-LGO (f_{BHLGO}), LGO-LGO (f_{LGOLGO}), LGO-NS (f_{LGONS}), BH-BH (f_{BHBH}), BH-NS (f_{BHN}), NS-NS (f_{NSNS}) binaries, BH-BH binaries with $m_{\text{bin}} > 130 M_{\odot}$ (f_{M130}), and the total number of mergers (N_{mer}), where LGOs represent lower mass gap objects with masses in $2-5 M_{\odot}$.

| input | | output | | | | | | | |
|-------|-------------------------------------|--------------------|---------------------|--------------------|-------------------|--------------------|--------------------|-------------------|-------------------|
| Model | Parameter | f_{BHLGO} | f_{LGOLGO} | f_{LGONS} | f_{BHBH} | f_{BHN} | f_{NSNS} | f_{M130} | N_{mer} |
| M1 | Fiducial | 4×10^{-3} | 3×10^{-4} | 3×10^{-4} | 0.989 | 6×10^{-3} | 3×10^{-4} | 0.03 | 1.6×10^3 |
| M2 | $m_{1\text{gBH}} \leq 45 M_{\odot}$ | 7×10^{-4} | 5×10^{-5} | 7×10^{-5} | 0.998 | 1×10^{-3} | 5×10^{-5} | 0.11 | 2.0×10^3 |
| M3 | $\Gamma_{\text{Edd,cir}} = 20$ | 5×10^{-3} | 5×10^{-5} | 9×10^{-5} | 0.994 | 8×10^{-4} | 5×10^{-5} | 0.35 | 1.9×10^3 |

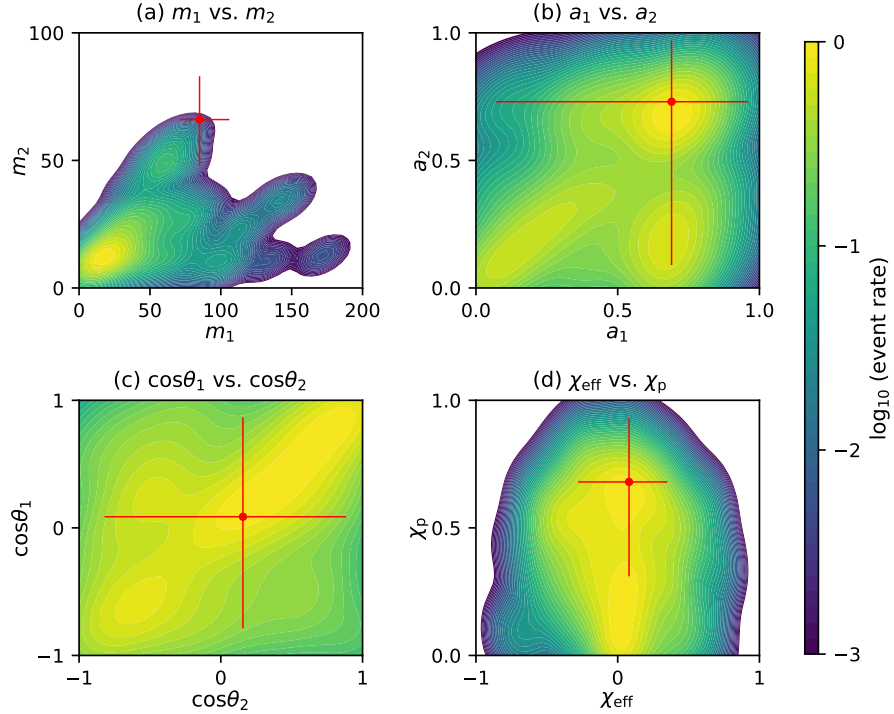


Figure 1. The parameter distributions for merging binaries weighted by the detectable volume at $t = 10$ Myr in model M1. The four panels present distributions of (a) the masses of primary and secondary object (m_1 vs. m_2) in units of M_{\odot} , (b) the dimensionless spins of primary and secondary objects (a_1 vs. a_2), (c) the angles between the binary orbital angular momentum and the BH spins ($\cos\theta_1$ and $\cos\theta_2$), and (d) the mass-weighted sum of the individual spin components perpendicular to the orbital plane (χ_{eff}) vs. the precession parameter (χ_p), respectively. The error bars correspond to the 90 percentile credible intervals inferred in GW190521 (The LIGO Scientific Collaboration et al. 2020b).

star formation in strong gravitational field (e.g. Nayakshin et al. 2007), gas accretion (e.g. Davies & Lin 2020), uncertainties in stellar evolution (e.g. Belczynski et al. 2010), and the diversity in the possible origin of objects (e.g. Mapelli & Gualandris 2016).

In model M3, we increase the maximum accretion rate in Eddington units onto stellar-mass COs to 20, given the uncertainties due to radiation feedback onto dust (Toyouchi et al. 2020) and rotating gas (Jiang et al. 2014; Sugimura et al. 2018), and the possible anisotropy of radiation (Proga et al. 2000).

3. RESULTS

3.1. Upper mass-gap mergers

We first compare the properties of predicted mergers in AGN disks with those of the upper-mass gap event GW190521. The parameter distributions for all events

at $t = 10$ Myr in model M1 are shown in Fig. 1, while those for specific generation mergers at $t = 100$ Myr reproducing well GW190521 in models M1–M3 in Fig. 2. Note that the maximum binary masses are not sensitive to time in later phases of $t \geq 10$ Myr as discussed in the Appendix. In Fig. 2, results at $t = 100$ Myr are presented to reduce variation due to a small number of mergers. The distributions are weighted by the observable volume depending on the masses of merging binaries calibrated for aLIGO Handford prior to O3 as in Paper I, while the dependence on either χ_{eff} or eccentricity is ignored in terms of detection volume for simplicity. The plots are smoothed by performing kernel-density estimate using Gaussian kernels whose bandwidth is chosen to satisfy Scott's rule (Scott 1992).

In model M1, the primary-mass distribution extends to as high as $> 100 M_{\odot}$ despite the low initial BH mass

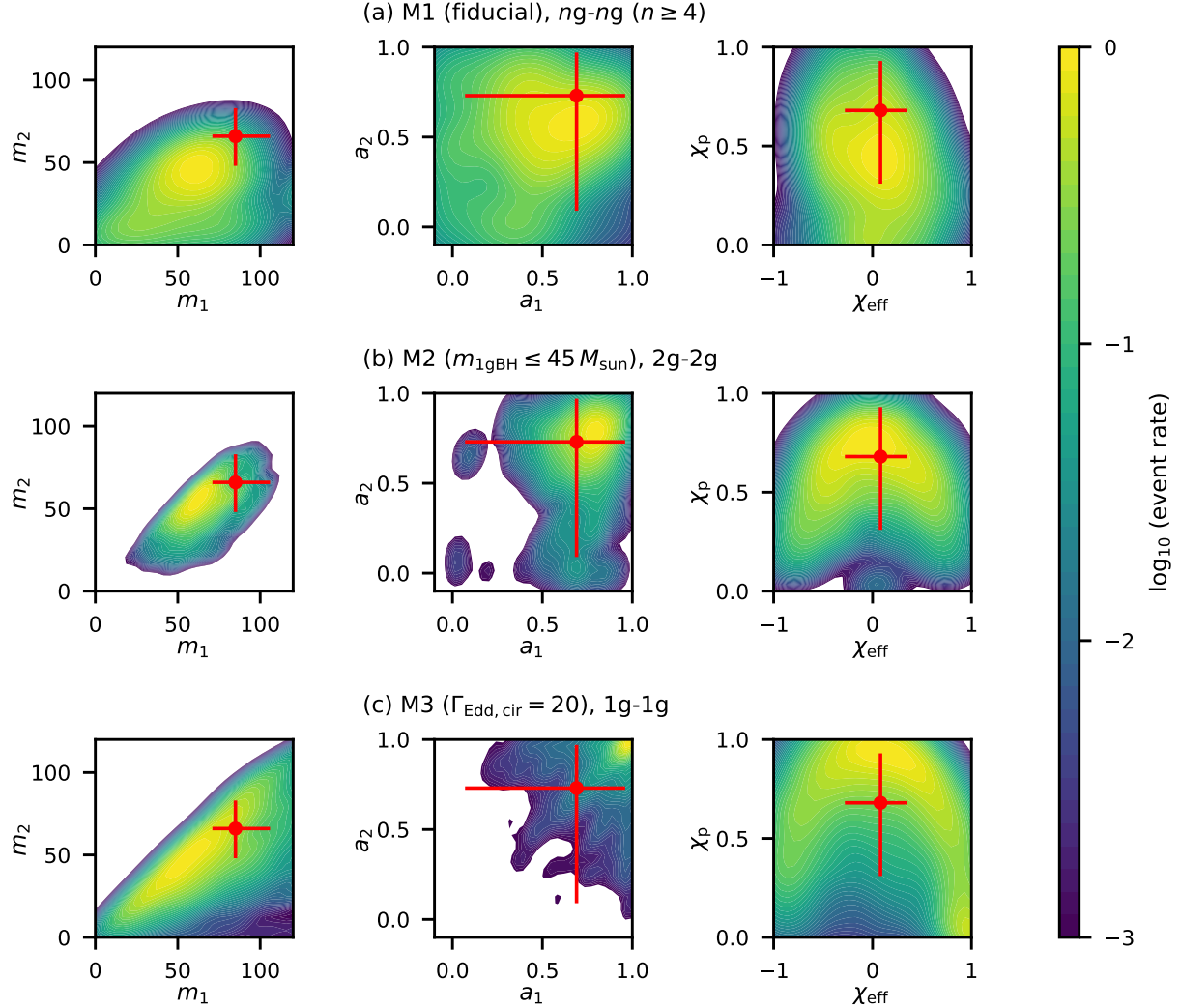


Figure 2. The parameter distributions for merging binaries weighted by the detectable volume among ng - ng mergers with $n \geq 4$ in model M1 (a), 2g-2g mergers in model M2 (b), and 1g-1g mergers in model M3 (c), where ng BHs represent BHs consisted of merged n -1g BHs. Left, middle, and right panels show the distributions of m_1 vs. m_2 in units of M_\odot , and the dimensionless spin parameters a_1 vs. a_2 , and χ_{eff} vs. χ_p , respectively. The error bars correspond to the 90 percentile credible intervals for GW190521 (The LIGO Scientific Collaboration et al. 2020b).

of $\leq 15 M_\odot$ (Fig. 1 a). High-mass events with $\gtrsim 50 M_\odot$ BHs, including GW190521, primarily arise from high-g mergers as seen in Fig. 2 a, where the distribution is shown for the mergers between high n -generation objects with $n \geq 4$. In model M1 at $t = 10$ Myr, the expected detection fraction of upper-mass gap mergers with $50 M_\odot \leq m_1 \leq 150 M_\odot$ contributed by 3, 4, 5, 6, 7, 8, and $n \geq 9$ th-generation primary BHs is 0, 5, 17, 30, 21, 3, and 24 percent, respectively, where an ng BH signifies a BH consisted of n 1g BHs as the merged progenitors. As the mass of ng BHs is at most $\sim n \times 15 M_\odot$ in model M1, primary BHs of GW190521-like mergers $m_1 \sim 85 M_\odot$ come from $n \geq 6$ -g BHs. The fraction of massive binary mergers with $m_{\text{bin}} \geq 130 M_\odot$ (~ 90 percentile lower limit for GW190521) over all events (f_{M130}) is 0.03 in model M1. Since GW190521 was found among

~ 60 triggers, the rate of this type of events can be explained by the AGN channel if it is the dominant channel for all the detected events. Here, note that the maximum mass of merging binaries ($\sim 185 M_\odot$) is significantly reduced from Papers I ($\sim 10^4 M_\odot$), which is discussed in the Appendix.

The mergers tend to have high spin around ~ 0.7 (Fig. 1 b). This is because the spin of their members is already high as a result of previous episode of mergers (e.g. Buonanno et al. 2008). Also, the angles θ_1, θ_2 between the binary orbital angular momentum and the primary and secondary BH spin, respectively, are widely distributed in the entire range of $(0-\pi)$ (Fig. 1 c) due to several BS interactions, which are assumed to randomize the orientation of the orbital angular momentum. Yet, strong correlation between θ_1 and θ_2 is still observed owing

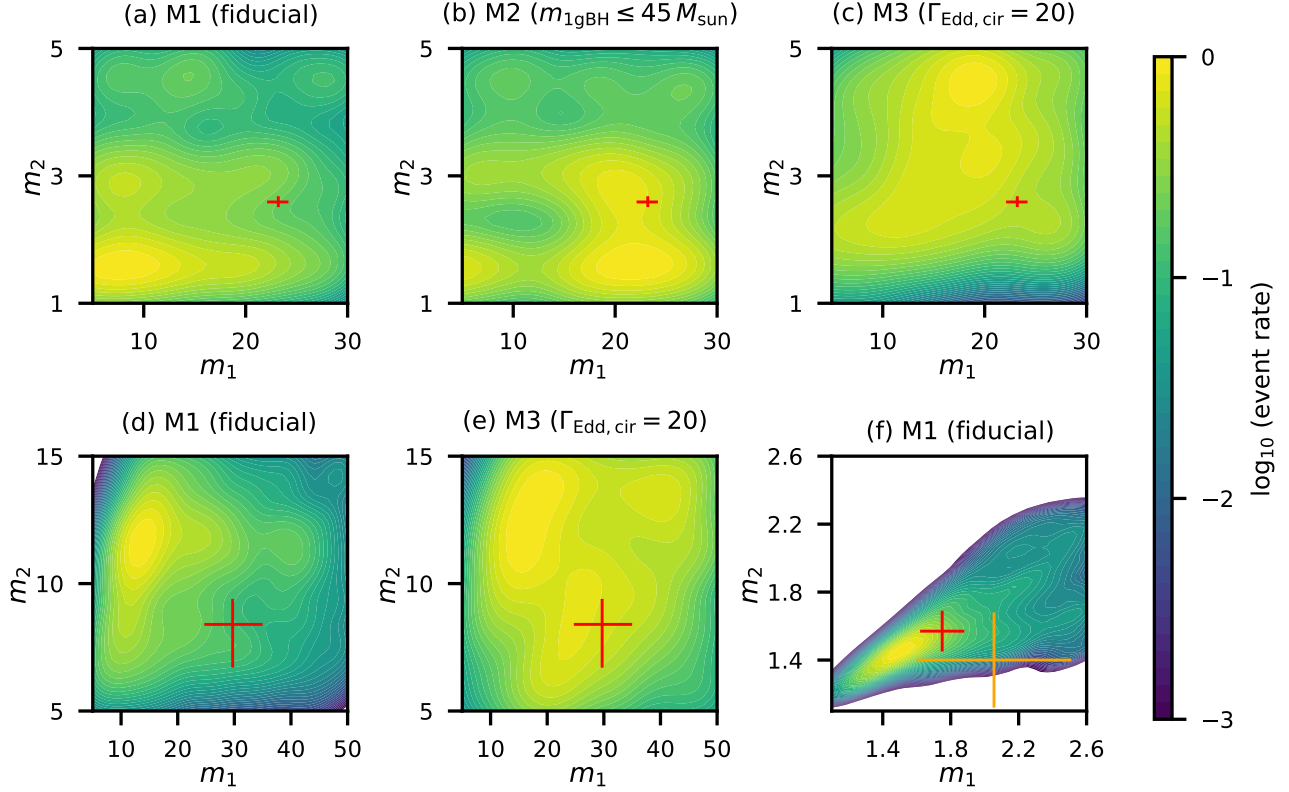


Figure 3. The distribution of m_1 and m_2 in units of M_\odot weighted by the detectable volume in models M1–M3 at $t = 100$ Myr. The error bars correspond to the 90 percentile credible intervals for GW190814 (panels a–c, Abbott et al. 2020b), GW190412 (panels d and e, The LIGO Scientific Collaboration et al. 2020a), and GW190425 (panel f, Abbott et al. 2020a) for low-(red) and high-(orange) spin priors.

ing to spin alignment by gas accretion. High-g mergers have a wide range of χ_p and χ_{eff} (right panel of Fig. 2 a) due to the spin enhancement during mergers and the randomization of the orbital angular momentum directions by BS interactions.

In summary, the results above demonstrate that mergers between high-g BHs in model M1 is consistent with the observed properties (χ_{eff} , χ_p , m_1 , m_2 , a_1 , a_2 , θ_1 , θ_2 , rate) of GW190521.

Fig. 2b shows the parameter distributions of the 2g-2g BH mergers in model M2, in which the maximum initial BH mass is elevated to $45 M_\odot$, typical for metal-poor progenitors. This high initial mass allows 2g-2g BH mergers to reach the mass range of GW190521. The fraction of mergers with $m_{\text{bin}} \geq 130 M_\odot$ becomes as high as 0.11 in this model. Since some stars in NSCs are indeed metal-poor (Do et al. 2020), the observed rate of GW190521-like events is in concordance also with model M2 as long as the AGN channel comprises at least $\sim 15\%$ of all the GW events detected to date. This number is calculated from the observed massive merger fraction ($\sim 1/60$) divided by the fraction in our model (0.11).

Fig. 2c shows the results for the 1g-1g mergers in model M3, in which the accretion rate can be as high as 20 times the Eddington accretion rate. Now, owing to rapid growth by accretion, even some 1g-1g mergers reach the mass range of GW190521. The gas accretion also significantly enhances the BH spin, and a_1 , a_2 , and χ_p (or $|\chi_{\text{eff}}|$). Such rapid accretion scenario may be fa-

vored by the presence of events with high $|\chi_{\text{eff}}|$ values such as $\chi_{\text{eff}} = 0.81_{-0.21}^{+0.15}$ of GW151216 (Zackay et al. 2019b). Precise estimate for the BH spins in future will further constrain its validity.

In conclusion, the binary property, including the mass, spin and occurrence rate, of GW190521 is consistent with the events via the AGN channel. In particular, its origin can be well explained either by high(≥ 4)-g merger of massive BHs, by 2g BH mergers which have massive low-metallicity progenitor stars, or by mergers of BHs that have rapidly grown by super-Eddington accretion.

3.2. lower mass-gap, low mass-ratio, and massive NS mergers

Next, we examine whether our model can reproduce lower mass-gap, low mass-ratio, and massive NS merger events, like GW190814, GW190412, and GW190425, respectively. Fig. 3 shows the mass distribution of the merging objects for models M1–M3. The mass ranges shown in each panel is chosen so that the distribution around the corresponding observed events is clearly seen. We do not show the result of model M2 for GW190412 since the initial BH mass falls in the range 15 – $45 M_\odot$ by construction and thus is in contradiction with the secondary mass of the event ($m_2 = 8.4_{-1.0}^{+1.7} M_\odot$).

In models M1–M3, moderate probability ($f_{\text{BHLGO}} = 0.07$ – 0.4% , Table 1) of the detection fraction is predicted for mergers between LGOs and BHs. Note that f_{BHLGO} can be as high as $\gtrsim 1\%$ depending on the adopted pa-

rameters (see Appendix). This is marginally consistent with the rate of events like GW190814, which was found from ~ 60 triggers in LIGO/Virgo observations, provided the AGN channel is the dominant channel for all the detected GW events. Secondary objects of around $2.6 M_{\odot}$ can be produced by mergers of NSs (panels a and b), while in model M3, 1g objects can be as massive as this thanks to super-Eddington accretion. With low spin magnitude ($\lesssim 0.07$, Abbott et al. 2020b), the primary BH of GW190814 is probably 1g and has hardly grown by accretion. This fact favors a merger between a massive-1g BH and a LGO as the origin of GW190814 as in model M2.

Mergers like GW190412, having the low mass-ratio ($q = 0.28^{+0.13}_{-0.07}$) and the high primary-BH spin ($a_1 = 0.43^{+0.16}_{-0.26}$), can be explained by 2g-1g mergers in model M1 (panel d of Fig. 3) and by 1g-1g mergers in model M3 (panel e). The detection probability of 2g-1g mergers is $\sim 16\%$ in model M1, while that for low mass-ratio mergers with $q < 0.3$ is $\sim 8\%$ in model M3. Also, non-zero spin for the primary BH in GW190412 may be consistent with being 2g (or high-g) as in model M1, or experienced significant accretion as in model M3.

Overall, the properties of GW190814/GW190412 can be explained by the AGN channel either by mergers among 2g-1g objects or mergers of BHs grown by super-Eddington accretion. The possible $1g-20 M_{\odot}$ BH of GW190814 prefers moderately metal-poor progenitors. GW190412 allows for solar-metallicity progenitors because high mass of the primary BH ($\sim 30 M_{\odot}$) suggests it to be a 2 or higher-g object or growth by significant accretion. As both high- and low-metallicity stars are present in NSCs (Do et al. 2020), AGN disks can provide candidate sites for both events.

Finally, the massive NS merger event GW190425 is well reproduced by growth of the progenitors by gas accretion in model M1 at $t = 100$ Myr (panel f of Fig. 3). This result is consistent with the finding in Yang et al. (2020b) that gas accretion expected in the AGN channel can produce GW190425-like massive NS mergers. In model M1, the merging NS mass extends to $\sim 1.6 M_{\odot}$ at $t = 10$ Myr, slightly lower than the CO masses of GW190425. Since the mass accreted in a fixed time interval is roughly proportional to the gas accretion rate, which is here set to the Eddington rate with 10% radiative efficiency, the mass distribution of NS mergers can constrain the typical accretion rate onto the progenitor and the AGN disk lifetime once a large number of NS mergers in AGNs are observed. However, the detection fraction of NS-NS mergers over all mergers is $f_{\text{NSNS}} \sim 5 \times 10^{-5} - 3 \times 10^{-3}$ (Table 1, see also Appendix), which is much lower than the actual observed fraction ($\sim 1/30$). Therefore, it might be unlikely that GW190425 is originated from AGNs.

We have also calculated several models with different sets of the parameters related to the properties of the AGN disk, BH population, etc. and found that the fraction of mass-gap mergers is only moderately affected by the difference in their choice (see Appendix).

4. CONCLUSIONS

In this *Letter*, we have followed the evolution of compact objects in AGN disks by way of one-dimensional N -body simulations, combined with semi-analytical prescriptions incorporating gaseous and stellar interactions,

by extending our previous model to include not only black holes but also neutron stars. We have then compared the expected properties of compact-object mergers in AGN disks with those of the observed events GW190521, GW190814, GW190412, and GW190425.

Our main findings are summarized as follows:

1. The AGN channel can produce high BH-mass mergers like GW190521 in multiple ways: (i) mergers among high-g BHs, (ii) mergers of 2g-2g BHs with metal-poor progenitors, or (iii) mergers of BHs which have acquired mass via moderately super-Eddington accretion. Events with roughly equal-mass ratio are expected in this channel, unlike those occurring in the migration traps of the AGN disks.
2. Mergers in the lower mass-gap or with unequal masses like GW190814 and GW190412 can be explained in the AGN channel by 2g-1g mergers or 1g-1g mergers with significant gas accretion, with moderate occurrence probability.
3. The Massive neutron-star merger GW190425 can be explained by the AGN channel if the progenitors had acquired significant mass via accretion, although the predicted rate is much lower than the observed rate.

The authors thank Will Farr for useful suggestions. This work is financially supported by the Grants-in-Aid for Basic Research by the Ministry of Education, Science and Culture of Japan (HT:17H01102, 17H06360, KO:17H02869, 17H01102, 17H06360). ZH acknowledges support from NASA grant NNX15AB19G and NSF grants 1715661 and 2006176. This work received funding from the European Research Council (ERC) under the European Union’s Horizon 2020 Programme for Research and Innovation ERC-2014-STG under grant agreement No. 638435 (GalNUC) (to BK). J.S. is supported by the European Unions Horizon 2020 research and innovation programme under the Marie Skłodowska-Curie grant agreement No. 844629. IB acknowledges support from the Alfred P. Sloan Foundation and from the University of Florida. Simulations and analyses were carried out on Cray XC50 and computers at the Center for Computational Astrophysics, National Astronomical Observatory of Japan.

REFERENCES

Abbott, B. P., Abbott, R., Abbott, T. D., et al. 2019, *Physical Review X*, **9**, 031040
 —. 2020a, *ApJ*, **892**, L3
 Abbott, R., Abbott, T. D., Abraham, S., et al. 2020b, *ApJ*, **896**, L44
 —. 2020c, arXiv e-prints, arXiv:2010.14527
 —. 2020d, *ApJ*, **900**, L13
 Bartos, I., Kocsis, B., Haiman, Z., & Márka, S. 2017, *ApJ*, **835**, 165
 Belczynski, K., Bulik, T., Fryer, C., et al. 2010, *ApJ*, **714**, 1217
 Belczynski, K., Bulik, T., Olejak, A., et al. 2018, arXiv e-prints, arXiv:1812.10065
 Bellovary, J. M., Mac Low, M. M., McKernan, B., & Ford, K. E. S. 2016, *ApJ*, **819**, L17
 Buonanno, A., Kidder, L. E., & Lehner, L. 2008, *Phys. Rev. D*, **77**, 026004
 Chatzopoulos, E., & Wheeler, J. C. 2012, *ApJ*, **748**, 42

Chen, Y., Bressan, A., Girardi, L., et al. 2015, *MNRAS*, **452**, 1068

Czerny, B., Wang, J.-M., Du, P., et al. 2019, *ApJ*, **870**, 84

Davies, M. B., & Lin, D. N. C. 2020, *MNRAS*, [arXiv:2008.10033](https://arxiv.org/abs/2008.10033) [[astro-ph.GA](#)]

Dietrich, T., Ujevic, M., Tichy, W., Bernuzzi, S., & Brügmann, B. 2017, *Phys. Rev. D*, **95**, 024029

Do, T., David Martinez, G., Kerzendorf, W., et al. 2020, *ApJ*, **901**, L28

Farmer, R., Renzo, M., de Mink, S. E., Marchant, P., & Justham, S. 2019, *ApJ*, **887**, 53

Fragione, G., Grishin, E., Leigh, N. W. C., Perets, H. B., & Perna, R. 2019, *MNRAS*, **488**, 47

Fryer, C. L., Belczynski, K., Wiktorowicz, G., et al. 2012, *ApJ*, **749**, 91

Fuller, J., & Ma, L. 2019, *ApJ*, **881**, L1

Gayathri, V., Healy, J., Lange, J., et al. 2020, arXiv e-prints, [arXiv:2009.05461](https://arxiv.org/abs/2009.05461)

Gerosa, D., Mould, M., Gangardt, D., et al. 2020a, arXiv e-prints, [arXiv:2011.11948](https://arxiv.org/abs/2011.11948)

Gerosa, D., Vitale, S., & Berti, E. 2020b, arXiv e-prints, [arXiv:2005.04243](https://arxiv.org/abs/2005.04243)

Graham, M. J., Ford, K. E. S., McKernan, B., et al. 2020, *Phys. Rev. Lett.*, **124**, 251102

Greene, J. E., & Ho, L. C. 2007, *ApJ*, **667**, 131

Hopkins, P. F., Hernquist, L., Cox, T. J., et al. 2005, *ApJ*, **630**, 705

Hopman, C., & Alexander, T. 2006, *ApJL*, **645**, L133

Jiang, Y.-F., Stone, J. M., & Davis, S. W. 2014, *ApJ*, **796**, 106

Kimball, C., Talbot, C., Berry, C. P. L., et al. 2020, arXiv e-prints, [arXiv:2011.05332](https://arxiv.org/abs/2011.05332)

Leigh, N. W. C., Geller, A. M., McKernan, B., et al. 2018, *MNRAS*, **474**, 5672

Levin, Y. 2007, *MNRAS*, **374**, 515

Madau, P., & Dickinson, M. 2014, *ARA&A*, **52**, 415

Mapelli, M., & Gualandris, A. 2016, Star Formation and Dynamics in the Galactic Centre, Vol. 905 (Lecture Notes in Physics, Springer, Cham), 205

McKernan, B., Ford, K. E. S., Bellovary, J., et al. 2018, *ApJ*, **866**, 66

McKernan, B., Ford, K. E. S., Bartos, I., et al. 2019, *ApJ*, **884**, L50

Nayakshin, S., Cuadra, J., & Springel, V. 2007, *MNRAS*, **379**, 21

Nitz, A. H., & Capano, C. D. 2020, arXiv e-prints, [arXiv:2010.12558](https://arxiv.org/abs/2010.12558)

O’Leary, R. M., Kocsis, B., & Loeb, A. 2009, *MNRAS*, **395**, 2127

O’Leary, R. M., Meiron, Y., & Kocsis, B. 2016, *ApJ*, **824**, L12

Ozel, F., Psaltis, D., Narayan, R., & Santos Villarreal, A. 2012, *ApJ*, **757**, 55

Proga, D., Stone, J. M., & Kallman, T. R. 2000, *ApJ*, **543**, 686

Safarzadeh, M., & Haiman, Z. 2020, arXiv e-prints, [arXiv:2009.09320](https://arxiv.org/abs/2009.09320)

Samsing, J., Bartos, I., D’Orazio, D. J., et al. 2020, arXiv e-prints, [arXiv:2010.09765](https://arxiv.org/abs/2010.09765)

Scott, D. 1992, Multivariate Density Estimation: Theory, Practice, and Visualization, A Wiley-interscience publication (Wiley)

Shankar, F., Weinberg, D. H., & Miralda-Escudé, J. 2013, *MNRAS*, **428**, 421

Stone, N. C., Metzger, B. D., & Haiman, Z. 2017, *MNRAS*, **464**, 946

Sugimura, K., Hosokawa, T., Yajima, H., Inayoshi, K., & Omukai, K. 2018, *MNRAS*, **478**, 3961

Szolgyen, A., & Kocsis, B. 2018, *Phys. Rev. Lett.*, **121**, 101101

Tagawa, H., Haiman, Z., Bartos, I., & Kocsis, B. 2020a, *ApJ*, **899**, 26

Tagawa, H., Haiman, Z., & Kocsis, B. 2020b, *ApJ*, **898**, 25

Tagawa, H., Kocsis, B., Haiman, Z., et al. 2020c, arXiv e-prints, [arXiv:2010.10526](https://arxiv.org/abs/2010.10526)

The LIGO Scientific Collaboration, the Virgo Collaboration, Abbott, R., et al. 2020a, arXiv e-prints, [arXiv:2004.08342](https://arxiv.org/abs/2004.08342)

—. 2020b, arXiv e-prints, [arXiv:2009.01075](https://arxiv.org/abs/2009.01075)

—. 2020c, arXiv e-prints, [arXiv:2010.14533](https://arxiv.org/abs/2010.14533)

Thompson, T. A., Quataert, E., & Murray, N. 2005, *ApJ*, **630**, 167

Tiwari, V., & Fairhurst, S. 2020, arXiv e-prints, [arXiv:2011.04502](https://arxiv.org/abs/2011.04502)

Toyouchi, D., Hosokawa, T., Sugimura, K., & Kuiper, R. 2020, *MNRAS*, **496**, 1909

Yang, Y., Bartos, I., Haiman, Z., et al. 2019, *ApJ*, **876**, 122

Yang, Y., Gayathri, V., Bartos, I., et al. 2020a, arXiv e-prints, [arXiv:2007.04781](https://arxiv.org/abs/2007.04781)

—. 2020b, arXiv e-prints, [arXiv:2007.04781](https://arxiv.org/abs/2007.04781)

Zackay, B., Dai, L., Venumadhav, T., Roulet, J., & Zaldarriaga, M. 2019a, arXiv e-prints, [arXiv:1910.09528](https://arxiv.org/abs/1910.09528)

Zackay, B., Venumadhav, T., Dai, L., Roulet, J., & Zaldarriaga, M. 2019b, *Phys. Rev. D*, **100**, 023007

APPENDIX

ALTERNATIVE MODELS

In this section, we present the parameter dependence of the results using a total of 22 different models, listed in Table 2. We also discuss merging mass distributions in the AGN channel.

MERGERS IN UPPER-MASS GAP

We find that the fraction of mergers of massive binaries of $\geq 130 M_{\odot}$ (f_{M130}) is zero when the BH number in inner regions ($r \lesssim 0.01$ pc) of the AGN disk is low due to the small size of the AGN disk (model M4), the high velocity dispersion of BHs (models M5, M16), no radial migration (model M7), low mass for NSCs (model M14), shallow density profile of BHs (model M15), or short duration of an AGN phase ($t = 1$ Myr, model M1). On the other hand, f_{M130} is enhanced if the initial masses of 1g BHs are massive (model M2), super-Eddington accretion is allowed (model M3), large number of BHs initially exists (model M13), or BHs can efficiently migrate to inner regions of $r \lesssim 10^{-3}$ pc. In models M8–M11, the fraction of mergers in the inner regions ($r \lesssim 10^{-3}$ pc) is higher than that in model M1. In the inner regions, massive BHs can merge with high binary eccentricity due to GW-capture binary formation (see Paper III), which may be consistent with possible high eccentricity in GW190521 implied by [Gayathri et al. \(2020\)](#).

Here, the maximum masses of merging binaries in the fiducial model ($\sim 185 M_{\odot}$) are significantly reduced from those in Papers I ($\sim 10^4 M_{\odot}$). This is due to the exchange interactions and disruption of softer binaries during binary-binary interactions, which are not included previously. With the exchanges included, both the number and maximum mass of mergers become smaller, because massive objects are retained in binaries after the exchanges and the more energy must be extracted for the more massive binaries to merge, during which many lighter COs receive strong kicks, reducing the number of COs in AGN disks.

Also, in our fiducial model, mergers between two high-generation BHs are common and the majority of them have high mass-ratio close to unity, as is the case for GW190521. Such high-g-high-g mergers do not occur in the model by [Yang et al. \(2019\)](#), who assumed that mergers occurs in the migration traps shortly after being captured in the disk. In that case, runaway growth of a single object by ng -1g mergers took place instead. In AGN disks outside the migration traps, high-g-high-g mergers can be more frequent because of the following reasons: (i) it takes longer for binary hardening and merger, (ii) objects kicked out from the disk by BS interactions interact less with others, and (iii) different objects orbit and merge at different distances from the SMBH due to variations in initial positions,

gap-opening regions, and migration speeds. Combinations of these enable objects to avoid merging into one massive object in contrary to mergers in the migration traps.

In the fiducial model, at $t = 1, 10$, and 100 Myr, respectively, the maximum masses of merging binaries are $130, 185$, and $185 M_{\odot}$, and the numbers of mergers are $260, 1, 600$, and $7, 300$, if the AGN disk exists for these durations. Thus, the merger rate decreases with time, as the rate of new BH captures in the disk by gas dynamical friction decreases. This is because of the strong dependence of the capture timescale on the initial CO velocity relative to the local AGN disk gas motion ($\propto v_{\text{ini}}^4$, Eq. 26 in paper I). COs having low v_{ini} are quickly captured, while those with high v_{ini} are typically not captured by the AGN disk within 100 Myr. Also, the maximum masses are not sensitive to disk lifetimes beyond $t \geq 10$ Myr. This is because mergers become infrequent and massive BHs often migrate to the inner boundary. Here, the number of BHs that migrate to the inner boundary of $r = 10^{-4}$ pc is ~ 90 at $t = 100$ Myr, while it is ~ 10 at $t = 10$ Myr. Note that objects which reach $r \leq 10^{-4}$ pc are not followed in our model, and are instead removed from the simulation. In these regions, COs may merge with each other if they accumulate in migration traps (Bellovary et al. 2016) or they may accrete onto the SMBH and observed by LISA as the migration timescale due to GW emission is comparable to the AGN lifetime (~ 30 Myr $(r/10^{-4}$ pc) $^4 (M_{\text{SMBH}}/4 \times 10^6 M_{\odot})^{-2} (m_{\text{CO}}/100 M_{\odot})^{-1}$, where M_{SMBH} and m_{CO} are the SMBH and the CO masses). Note that as massive BHs are rare, the evolution of maximum masses likely suffers some variations. For example, with an independent realization of the initial condition, the maximum masses of merging binaries are $70, 138$, and $186 M_{\odot}$, at $t = 1, 10$, and 100 Myr, respectively. In all cases, the growth of the maximum mass is slowed down in later phases.

In the fiducial model, f_{M130} decreases in $t \geq 10$ Myr due to inefficient capture of BHs in later phases and migration of massive BHs to the inner boundary of the AGN disk as discussed above. On the other hand, f_{M130} increases in $t \geq 10$ Myr in model M12 and M13, in which the gas accretion rate at the outer boundary is low ($M_{\text{out}} = 0.01$ and $0.001 M_{\text{Edd}}$). In addition, in model M12, the maximum mass of merging binaries increases with time as those are $46, 142, 228$, and $283 M_{\odot}$ at $t = 1, 10, 100$, and 1000 Myr, respectively. Thus, the maximum merging mass and f_{M130} evolve more in later phases for low M_{Edd} models compared to that in the fiducial model. These are due to the difference of the gas density of the AGN disk. Inefficient gaseous processes (capture to the AGN disk and migration) due to low gas density facilitate growth of BHs in later phases. Such low M_{out} cases may be more important for understanding properties of mergers in the AGN channel as the number of mergers from AGNs with low Eddington rates may dominate over those with high Eddington rates depending on the Eddington rate distribution of AGNs (Hopkins et al. 2005; Greene & Ho 2007; Shankar et al. 2013), which is uncertain. If the merger rate is dominated by AGNs with low Eddington rates, the rate is significantly influenced by the transition radius from a standard disk to advection-dominated accretion flow, which possibly comes to $\gtrsim 10^{-3}$ – 10^{-2} pc and affect merger processes for $M_{\text{out}} \lesssim 10^{-3} M_{\text{Edd}}$ (Eq. 3 of Czerny et al. 2019), although the typical value of the radius is uncertain (e.g. Czerny et al. 2019).

MERGERS IN LOWER MASS GAP

The fraction of BH-LGO mergers is enhanced by several effects. In model M4, we assume that COs initially exist within $r_{\text{out,BH}} = 0.03$ pc. This resembles the situation in which the size of the AGN disk is 0.03 pc. In this model, f_{BHLGO} is enhanced to 0.10 . In the inner regions of the AGN disk, the capture timescale of COs by the AGN disk is shorter. As a large fraction of NSs and BHs are rapidly captured, the ratio of the number of NSs over BHs in the AGN disk is high and accordingly the rates of NS-NS and BH-LGO mergers are also relatively high.

In model M5, in which the initial velocity dispersion of BHs and NSs is virial ($\beta_{\text{v,BH}} = \beta_{\text{v,NS}} = 1$), f_{BHLGO} is enhanced to 0.03 . As the initial velocity dispersion of BHs and NSs increases, the numbers of BHs and NSs in the AGN disks decrease. Then, binary NSs have a high probability to merge without interacting with BHs and experiencing exchange of binary components. The high velocity dispersion of BHs might be realized if the AGN phase begins before dynamics of NSCs is regulated by vector resonant relaxation e.g. due to randomization of orbits of COs by major merger of galaxies, or if NSCs have negligible rotation on average.

In models M6 and M7, we assume that NSs have already merged prior to the AGN phase. Such situation may be realized if the high rate of NS-NS mergers ($\sim 1000 \text{ Gpc}^{-3} \text{ yr}^{-1}$) inferred from GW observations are driven by isolated binary evolution (but see Belczynski et al. 2018) and such mergers are not prevented by soft-BS interactions in NSCs, or NS mergers are facilitated by the Kozai-Lidov mechanism (e.g. Fragione et al. 2019). To investigate the effects of this possibility, we assume that a fraction of NSs (f_{LGO}) already merged with NSs prior to the start of the AGN episode, and LGOs may have initial masses with $2.6 M_{\odot}$. We investigate a model with $f_{\text{LGO}} = 0.1$ (M6), which would present an upper limit as the rate of core-collapse supernovae is $\sim 10^5 \text{ Gpc}^{-3} \text{ yr}^{-1}$ (Madau & Dickinson 2014) and that of NS-NS mergers is ~ 100 – $4000 \text{ Gpc}^{-3} \text{ yr}^{-1}$ (Abbott et al. 2019). f_{BHLGO} is moderately enhanced to 0.01 for $f_{\text{LGO}} = 0.1$ from its value of 4×10^{-3} for $f_{\text{LGO}} = 0$. Thus, isolated binary evolution may contribute to the fraction of mergers in the lower mass gap (f_{BHLGO}) in the AGN channel.

In model M8, in which COs do not migrate toward the SMBH, f_{BHLGO} is higher as the probability that the NS binaries interact with BHs and the binary components are exchanged is reduced. The efficiency of migration of COs in AGN disks is uncertain, while it affects various properties of mergers in AGN disks. Thus, this process is worth investigating in more detail in future work to better understand the implications for mergers in AGN disks.

MERGING MASS DISTRIBUTION

Here, we discuss the merging mass distribution. As a large number of events are reported in LIGO/Virgo O3a (Abbott et al. 2020c), we can assess the consistency between predicted and observed distributions more precisely. Recently, The LIGO Scientific Collaboration et al. (2020c) and Tiwari & Fairhurst (2020) analyzed the LIGO/Virgo's O1-O3a data and reconstructed merging mass distributions. The LIGO Scientific Collaboration et al. (2020c) reconstructed the primary mass distribution by a superposition of a (broken) power law and 0-2 Gaussian distributions, while Tiwari & Fairhurst (2020) reconstructed the chirp mass distribution by a superposition of twelve Gaussian distributions, which can flexibly recover features of the mass distribution. The LIGO Scientific Collaboration et al. (2020c) suggested that the m_1 distribution is more consistent with a broken power law with a break at $m_1 \sim 40 M_{\odot}$, or a power law with a Gaussian feature peaking at $m_1 \sim 34 M_{\odot}$. Interestingly, Tiwari & Fairhurst (2020) identified four peaks in the chirp mass distribution at 8, 14, 26, and $45 M_{\odot}$, which are roughly separated by a factor of around two, possibly suggesting frequent hierarchical mergers. Here, high values for χ_p inferred for observed GW events (Gerosa et al. 2020a) may also support this scenario. As hierarchical mergers are presumably most frequent in the AGN channel, it would be interesting to check whether such features can be reproduced in our model.

In model M1, peak-like structures are less clear in the chirp mass distribution (Fig. 4 a) despite of frequent hierarchical mergers. On the other hand, as the merging mass distribution is significantly affected by the adopted initial mass function of BHs, we performed model M22 in which the initial masses of all 1g BHs are set to $10 M_{\odot}$. Such a spiky initial mass function may be allowed depending on prescriptions of stellar mass loss (Belczynski et al. 2010). In this model, peaks in the m_{chirp} distribution become much clearer (panels c and e), although the number of peaks is larger than that implied by Tiwari & Fairhurst (2020), due to the contribution of mergers among various generation BHs like 1g-2g or 2g-3g. This model predicts that further peaks might be detectable by observing a larger number of events. On the other hand, the contribution of mergers among 1g-2g or 2g-3g BHs is supposedly influenced by frequency of BS interactions, which depends on several parameters and processes, such as δ_{IMF} , $\beta_{v, \text{BH}}$, and the efficiency of migration due to gaseous torque. Also, some peaks become smooth and close to a power-law like shape if we adopt different initial mass functions for BHs as in model M1 (panel a) or as time passes (panels c and e). Observational errors on the chirp mass further make the merging mass distribution somewhat smoother. As properties of peaks are influenced by several parameters, uncertainties, and observational effects, the features inferred by Tiwari & Fairhurst (2020) might be reproduced.

Meanwhile, the m_1 distributions (Fig. 4 b, d, and e) look roughly similar to those reconstructed by The LIGO Scientific Collaboration et al. (2020c). Note that the errors on m_1 are typically much larger than that on the chirp mass, which presumably reduces peaks in the observed m_1 distribution (Fig. 4 d and f). Hence, there is a possibility that the AGN channel can explain the observed features of merging masses. To constrain the contribution from the AGN channel, quantitative comparisons would be required, which will be conducted in a following work.

Table 2

Same as Table 1, but results for all models. “No gas hardening” and “No gas migration” respectively represent the models in which the gaseous torques are neglected with respect to the evolution of the binary semi-major axis and the radial position of the binary center of mass within the AGN disk. “BS in 2D” and “BS in 2→3D” represents the models in which BS interactions occur in 2D and 2→3D space, respectively (Paper III).

| Model | Parameter | output | | | | | | | |
|-------|--|--------------------|---------------------|--------------------|-------------------|--------------------|--------------------|--------------------|-------------------|
| | | f_{BHLGO} | f_{LGOLGO} | f_{LGONS} | f_{BHBH} | f_{BHNS} | f_{NSNS} | f_{M130} | N_{mer} |
| M1 | Fiducial | 4×10^{-3} | 3×10^{-4} | 3×10^{-4} | 0.989 | 6×10^{-3} | 3×10^{-4} | 0.03 | 1.6×10^3 |
| M2 | $m_{1\text{gBH}} \times 3$ | 7×10^{-4} | 5×10^{-5} | 7×10^{-5} | 0.998 | 1×10^{-3} | 5×10^{-5} | 0.11 | 2.0×10^3 |
| M3 | $\Gamma_{\text{Edd,cir}} = 20$ | 5×10^{-3} | 5×10^{-5} | 9×10^{-5} | 0.994 | 8×10^{-4} | 5×10^{-5} | 0.35 | 1.9×10^3 |
| M4 | $r_{\text{out,BH}} = 0.03 \text{ pc}$ | 0.10 | 2×10^{-3} | 3×10^{-3} | 0.82 | 0.07 | 3×10^{-3} | 0 | 3.1×10^2 |
| M5 | $\beta_{\text{v,BH}} = \beta_{\text{v,NS}} = 1$ | 0.03 | 2×10^{-3} | 2×10^{-3} | 0.94 | 0.03 | 2×10^{-3} | 0 | 5.9×10^2 |
| M6 | $f_{\text{LGO}} = 0.1$ | 0.01 | 1×10^{-3} | 7×10^{-4} | 0.984 | 4×10^{-3} | 4×10^{-4} | 0.03 | 1.8×10^3 |
| M7 | $f_{\text{LGO}} = 0.01$ | 6×10^{-3} | 3×10^{-4} | 5×10^{-4} | 0.989 | 5×10^{-3} | 4×10^{-4} | 0.01 | 1.6×10^3 |
| M8 | No gas mig. | 0.02 | 1×10^{-3} | 2×10^{-3} | 0.95 | 0.03 | 2×10^{-3} | 0 | 7.1×10^2 |
| M9 | No gas hard. | 2×10^{-3} | 7×10^{-4} | 2×10^{-3} | 0.98 | 0.01 | 1×10^{-3} | 0.11 | 1.5×10^3 |
| M10 | $r_{\text{out,BH}} = 0.3 \text{ pc}$ | 8×10^{-3} | 7×10^{-4} | 1×10^{-3} | 0.98 | 0.01 | 8×10^{-4} | 0.09 | 1.0×10^3 |
| M11 | $M_{\text{out}} = \dot{M}_{\text{Edd}}$ | 6×10^{-3} | 2×10^{-4} | 5×10^{-4} | 0.988 | 5×10^{-3} | 4×10^{-4} | 0.06 | 1.7×10^3 |
| M12 | $\dot{M}_{\text{out}} = 0.01 \dot{M}_{\text{Edd}}$ | 2×10^{-3} | 5×10^{-4} | 6×10^{-4} | 0.992 | 4×10^{-3} | 7×10^{-4} | 0.01 | 8.9×10^2 |
| M13 | $\dot{M}_{\text{out}} = 0.001 \dot{M}_{\text{Edd}}$ | 3×10^{-3} | 0 | 4×10^{-4} | 0.98 | 0.02 | 1×10^{-3} | 0 | 3.1×10^2 |
| M14 | $M_{\text{SMBH}} = 4 \times 10^7 M_{\odot}$ | 8×10^{-3} | 2×10^{-4} | 4×10^{-4} | 0.98 | 7×10^{-3} | 3×10^{-4} | 0.07 | 1.6×10^3 |
| M15 | $\delta_{\text{IMF}} = 1.7$ | 1×10^{-3} | 1×10^{-4} | 1×10^{-4} | 0.997 | 1×10^{-3} | 1×10^{-4} | 0.09 | 8.3×10^3 |
| M16 | $M_{\text{star,3pc}} = 3 \times 10^6 M_{\odot}$ | 0.01 | 2×10^{-4} | 6×10^{-4} | 0.98 | 0.01 | 5×10^{-4} | 0 | 5.3×10^2 |
| M17 | $\gamma_{\rho,\text{BH}} = 1.5$ | 1×10^{-3} | 0 | 7×10^{-5} | 0.994 | 4×10^{-3} | 2×10^{-4} | 0 | 9.8×10^2 |
| M18 | $\beta_{\text{v,BH}} = 0.4$ | 9×10^{-3} | 1×10^{-3} | 2×10^{-3} | 0.97 | 0.01 | 1×10^{-3} | 0 | 1.2×10^3 |
| M19 | $\beta_{\text{v,NS}} = 0.2$ | 6×10^{-3} | 7×10^{-4} | 8×10^{-4} | 0.987 | 6×10^{-3} | 7×10^{-4} | 0.06 | 2.2×10^3 |
| M20 | BS in 2D | 3×10^{-3} | 1×10^{-4} | 6×10^{-4} | 0.987 | 9×10^{-3} | 3×10^{-4} | 0.07 | 4.6×10^3 |
| M21 | BS in 2→3D | 3×10^{-3} | 2×10^{-4} | 4×10^{-4} | 0.991 | 6×10^{-3} | 3×10^{-4} | 0.05 | 3.4×10^3 |
| M21 | BS in 2→3D | 3×10^{-3} | 2×10^{-4} | 4×10^{-4} | 0.991 | 6×10^{-3} | 3×10^{-4} | 0.05 | 3.4×10^3 |
| M22 | $m_{1\text{gBH}} = 10 M_{\odot}$ | 3×10^{-3} | 3×10^{-4} | 3×10^{-4} | 0.991 | 5×10^{-3} | 4×10^{-4} | 0.01 | 1.6×10^3 |
| M1 | $t = 1 \text{ Myr}$ | 4×10^{-3} | 3×10^{-4} | 9×10^{-4} | 0.986 | 8×10^{-3} | 8×10^{-4} | 0 | 2.6×10^2 |
| M1 | $t = 100 \text{ Myr}$ | 0.02 | 9×10^{-4} | 1×10^{-3} | 0.96 | 0.02 | 8×10^{-4} | 8×10^{-3} | 7.3×10^3 |
| M12 | $\dot{M}_{\text{out}} = 0.01 \dot{M}_{\text{Edd}}, t = 100 \text{ Myr}$ | 7×10^{-3} | 5×10^{-4} | 1×10^{-3} | 0.98 | 7×10^{-3} | 7×10^{-4} | 0.05 | 4.6×10^3 |
| M12 | $\dot{M}_{\text{out}} = 0.01 \dot{M}_{\text{Edd}}, t = 1 \text{ Gyr}$ | 4×10^{-3} | 2×10^{-3} | 6×10^{-3} | 0.92 | 0.03 | 3×10^{-3} | 0.07 | 1.7×10^4 |
| M13 | $\dot{M}_{\text{out}} = 0.001 \dot{M}_{\text{Edd}}, t = 100 \text{ Myr}$ | 3×10^{-3} | 4×10^{-4} | 5×10^{-4} | 0.993 | 3×10^{-3} | 4×10^{-4} | 4×10^{-3} | 2.2×10^3 |

Table 3
Fiducial values of our model parameters.

| Parameter | Fiducial value |
|---|--|
| Spacial directions in which BS interactions occur | isotropic in 3D |
| Number of temporary binary COs formed during a BS interaction | $N_{\text{int}} = 20$ |
| Initial BH spin magnitude | $ \mathbf{a} = 0$ |
| Angular momentum directions of circum-CO disks | $\hat{\mathbf{J}}_{\text{CCOD}} = \hat{\mathbf{J}}_{\text{AGN}}$ for single COs, $\hat{\mathbf{J}}_{\text{CCOD}} = \hat{\mathbf{J}}_{\text{bin}}$ for COs in binaries |
| Ratio of viscosity responsible for warp propagation over that for transferring angular momentum | $\nu_2/\nu_1 = 10$ |
| Alignment efficiency of the binary orbital angular momentum due to gas capture (Eq. 14 in Paper II) | $f_{\text{rot}} = 1$ |
| Mass of the central SMBH | $M_{\text{SMBH}} = 4 \times 10^6 M_{\odot}$ |
| Gas accretion rate at the outer radius of the simulation (5 pc) | $\dot{M}_{\text{out}} = 0.1 \dot{M}_{\text{Edd}}$ with $\eta = 0.1$ |
| Fraction of pre-existing binaries | $f_{\text{pre}} = 0.15$ |
| Power-law exponent for the initial density profile for BHs and NSs | $\gamma_{\rho, \text{BH}} = 0, \gamma_{\rho, \text{NS}} = -0.5$ |
| Initial velocity anisotropy parameter such that $\beta_{v, \text{BH}} v_{\text{kep}}(r)$ is the BH velocity dispersion | $\beta_{v, \text{BH}} = 0.2, \beta_{v, \text{NS}} = 0.4$ |
| Efficiency of angular momentum transport in the α -disk | $\alpha_{\text{SS}} = 0.1$ |
| Stellar mass within 3 pc | $M_{\text{star,3pc}} = 10^7 M_{\odot}$ |
| Stellar initial mass function slope | $\delta_{\text{IMF}} = 2.35$ |
| Angular momentum transfer parameter in the outer star forming regions (Eq. C8 in Thompson et al. 2005) | $m_{\text{AM}} = 0.15$ |
| Accretion rate in Eddington units onto stellar-mass COs with a radiative efficiency $\eta = 0.1$ | $\Gamma_{\text{Edd,cir}} = 1$ |
| Numerical time-step parameter | $\eta_t = 0.1$ |
| Number of radial cells storing physical quantities | $N_{\text{cell}} = 120$ |
| Maximum and minimum r for the initial CO distribution | $r_{\text{in,BH}} = 10^{-4} \text{ pc}, r_{\text{out,BH}} = 3 \text{ pc}$ |
| Initial number of BHs and NSs within 3 pc | $N_{\text{BH,ini}} = 2 \times 10^4, N_{\text{NS,ini}} = 5 \times 10^4$ |

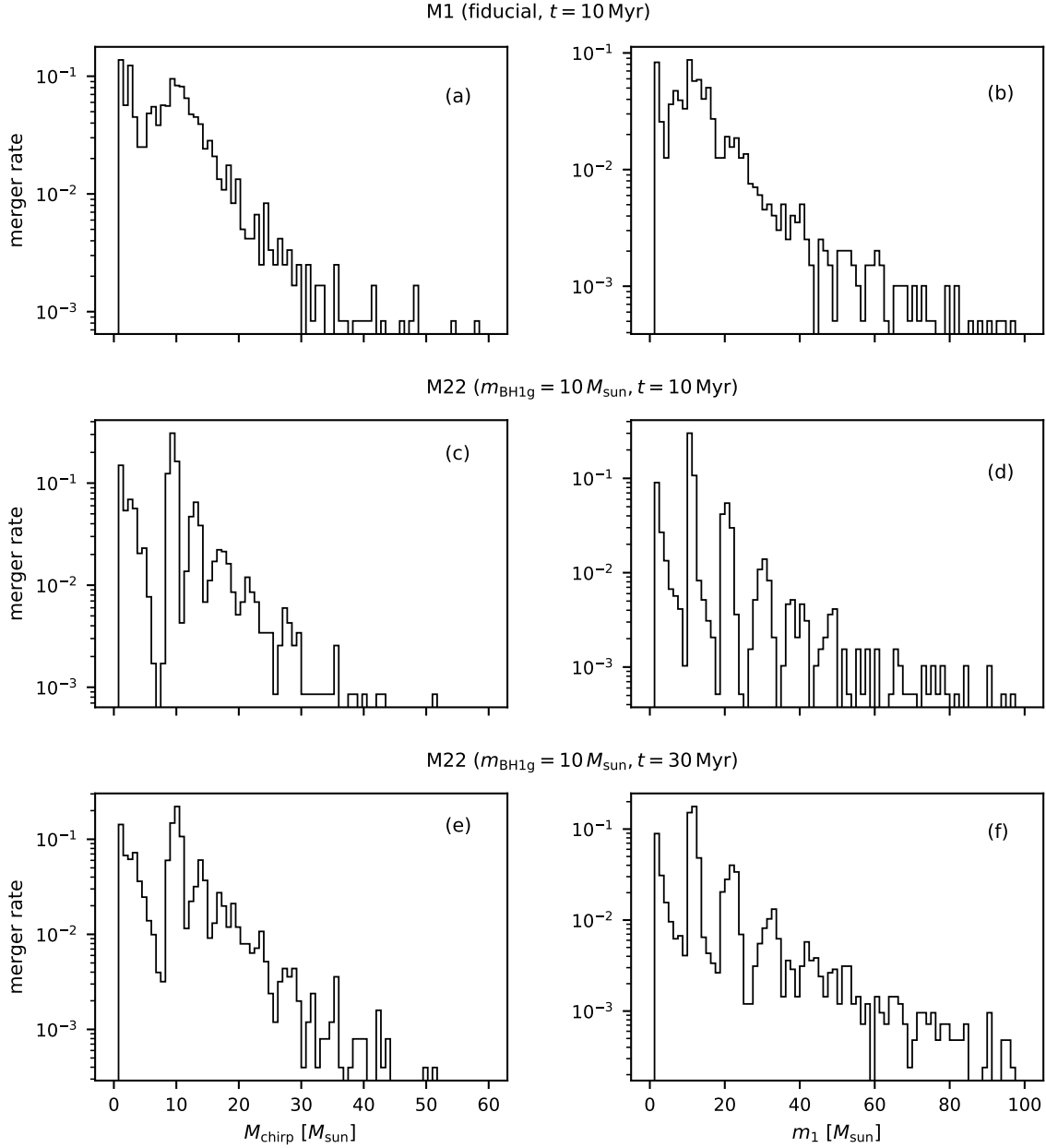


Figure 4. The distribution of the chirp (left) and primary (right) masses for model M1 at $t = 10$ Myr (panels a and b) and model M22 at $t = 10$ Myr (panels c and d) and $t = 30$ Myr (panels e and f).